J. Meas. Sci. Instrum., 2026, 17(1): 97-113.
DOI: 10.62756/jmsi.1674-8042.2026008
http://jmsi.publish.founderss.cn/
jmsi@nuc.edu.cn

Underwater image enhancement through cooperative optimization of color, detail, contrast and multi-scale fusion

CAO Rui, LI Bo, HU Hongping*, ZHANG Zhenwei, ZHU Xinchan
School of Mathematics, North University of China, Taiyuan 030051, China

***Corresponding author:** HU Hongping (hhp92@163.com)

Received: October 21, 2025 **Revised:** December 30, 2025 **Accepted:** January 5, 2026

Abstract: Due to the absorption and scattering of light in water, underwater images commonly exhibit degradation phenomena such as color cast, low visibility, and blurred details. In response to these issues, we propose a color, detail, contrast, and multi-scale fusion underwater image enhancement algorithm called CDCM. The algorithm first uses a color restoration method based on dark and bright channels to effectively correct color distortion of underwater images and restore their natural color balance. Secondly, utilizing morphological operations to enhance the contour and structural information of objects in the image so as to improve detail representation. In addition, the black eagle optimizer (BEO) is introduced and a new fitness function is designed to adaptively optimize image contrast. In the fusion stage, principal component weights are proposed and combined with other weighting strategies to achieve multi-scale image information fusion, enhancing the contrast while preserving rich textures and details. Experimental results on two real underwater image datasets UIEB and RUIE demonstrate that our method effectively reduces degradation phenomena, with image enhancement by improvements in color fidelity, contrast, and detail clarity compared to the existing methods. In terms of objective indicators, our method is also superior to other relevant methods, such as UCIQE, UIQM, AG, IE, PCQI, etc. Our work contributes to advancing underwater image processing techniques.

Key words: underwater image; color restoration; morphological transformation; black eagle optimizer (BEO); principal component weights; multi-scale fusion

0 Introduction

Abundant marine resources contain rich minerals, such as biological energy and chemical energy[1], which are crucial for maintaining the Earth's environment and supporting the sustainable development of human society. High-quality underwater images are essential for the study and management of marine resources[2]. However, images are frequently degraded because of light's attenuation and dispersion in water[3]. The attenuation of light causes red light with the longest wavelength to decay first and experience the most significant attenuation, whereas blue and green lights, with shorter wavelengths, are less affected by attenuation. Consequently, underwater images often exhibit blue-green color. In addition, light encounters particles in suspension as well as other substances in the water, causing scattering[5], which leads to low-contrast and blurry images. Capturing high-quality underwater images presents significant challenges, making it necessary to use computer vision technology to correct degraded images and improve their quality, serving subsequent analysis and processing.

Currently, most of underwater image restoration methods depend on underwater optical imaging models based on the physical models of underwater images[6-7]. These models account for the mechanism of degradation of underwater images and aim to improve image quality by estimating two key parameters: background light and transmission map. Researchers have employed various methods to estimate these parameters. For underwater optical imaging and atmospheric scatter models[8] that have similar mechanics. Dark channel prior (DCP) algorithm was proposed by He et al. [9] for underwater image restoration; a red channel prior method from Galdran et al. [10] used red channel information for estimation; a underwater dark channel prior method from Drews et al.[11] only considered green and blue channels and ignored red channel; a method called image blurriness and light absorption (IBLA) from Peng et al.[4] maked use of fuzzy priors and selective absorption properties of light for estimation; a study called generalization of underwater dark channel prior (GUDCP) from Liang et al.[13] estimated backscattered light through hierarchical search, using various prior knowledge to estimate transmission image;

and the method called nonconvex approach with structural priors (NASP) from Awan et al.[14] optimized the initial transmission map using a nonconvex energy function. Theorietically, underwater image restoration methods on the basis of physical models can accurately restore underwater images when environmental conditions and degradation parameters are known. In practical applications, since the environment is complex and changeable. while these techniques rely heavily on specific hypotheses and a previous set of knowledge, their generalization is limited.

On the contrary, the methods for the enhancement of underwater images based on non-physical models do not rely on specific imaging models. Such methods use computers to change the pixel values of images to achieve better underwater images. Typical methods include histogram equalization[15], white balance method[16], Retinex principle[17], and image fusion[18]. Lin et al.[19] designed a new factor for color adjustment, enriched details using two-scale separation, applied guided filtering to Retinex-based edge extraction, and finally joined the image using non-subsampled shearlet transform (NSST). Wang et al.[20] used channel similarity value as judgment standard, combined with statistical color correction method, to enhance the texture details of underwater images using wavelet decomposition. An et al.[21] used a hybrid fusion method to improve underwater images, eliminating color cast through a white balance correction module, enhancing low visibility via a visibility restoration module, improving hierarchical details using curve transformation, and ultimately resolving degradation issues through fusion enhancement. Zhang et al.[22] proposed a method to enhance the image by compensating three channels, enhancing global and local contrast, and finally fusing each version of the image to get the restored image. Since non-physical model based underwater enhancement is not constrained by presupposed conditions, it has high flexibility, adapting to all kinds of underwater images via rapid adjustment. However, due to the lack of consideration of the optical characteristics of underwater images, it is easy to introduce color deviations and the artifacts, leading to aggravated noise, over-saturation or under-saturation problems.

Currently, progress in underwater visual enhancement research has been driven by the rapid development of deep learning. Underwater image enhancement methods based on deep learning can be divided into two main types: convolutional neural networks (CNNs) based on hierarchical feature extraction architecture[23], and generative adversarial networks (GANs) based on generative and discriminative adversarial framework[24]. Li et al.[25] created a dataset called UIEB, using underwater images obtained from real photography to develope a network that achieves image enhancement through three different versions of images. Wu et al.[26] put forward a two-stage enhancement framework, called underwater image CNN based on structure decomposition (UWCNN-SD), decomposing the image into two different frequency components and then performing preliminary processing and refinement enhancements. Fu et al.[27] achieved underwater image enhancement by means of self-coding learning and sample prediction approach. Li et al.[28] put forward an un-supervised GAN for learning from underwater images and color correction. Consequently, the main areas of the image were located by using the transmission map, and a semantic importance compression module was also proposed to compress semantic information while retaining useful information. Finally, the image was reconstructed through the decoder. Wang et al.[29] suggested a network for underwater images, and red channel attention was optimized based on CycleGAN. Deep learning-based techniques for underwater image enhancement significantly improve the visual effects with strong feature extraction capability and better image quality. However, this requires a considerable number of training images from underwater, greatly limiting their adaptability to real underwater environments.

To response to the challenges of color distortion, low contrast, and lack of detail clarity of underwater images, we propose an image enhancement algorithm integrating color correction with multi-scale fusion.

The key contributions of our work are outlined as follows:

1) Color compensation based on dark and bright channels. By analyzing the color attenuation characteristics of underwater images, a background light discrimination method based on dark and bright channels is proposed, and a differentiated color compensation scheme is designed to overcome the limitations of traditional methods using fixed models so as to achieve more refined color restoration.

2) Morphological transformation detail enhancement. By separating bright pixels from dark pixels, foreground and background contours are enhanced respectively, thus optimizing detail representation. This method is rarely applied in traditional image enhancement and is an extension of existing methods.

3) Black eagle optimizer (BEO) contrast enhancement. Through global optimization search, the optimal contrast parameter is found based on fitness function, avoiding the local optimization problem of traditional methods and better adapting to the contrast requirements of different underwater images.

4) Multi-scale fusion and feature weight design. Unlike traditional wavelet or Gaussian Laplacian pyramid fusion methods, our algorithm introduces principal component analysis (PCA) weights and other feature weights to adjust fusion results so as to optimize the overall enhancement effect of the image, improving the balance and performance of different features.

The paper is arranged in this way: Section 1 delves into the theoretical underpinnings, providing a comprehensive exploration; Section 2 introduces an algorithm for enhancing underwater images, which leverages color restoration techniques and multi-scale fusion; In section 3, the experimental outcomes are discussed, encompassing both subjective evaluations and objective analyses; Finally, Section 4 draws together the findings of the study and makes conclusions.

1 Basic theory

The DCP theory is based on the statistical idea of many outdoor clear images. Most pixels in high-definition outdoor scenes have at least one color-channel with a very low level of brightness in their neighborhood, it can be approximated to 0, that is,

$$J^{\text{dark}}=\min_{y\in\Omega(x)}\left(\min_{c\in\{\text{R,G,B}\}}(J^c(y))\right)\to 0, \tag{1}$$

where J^{dark} is the dark channel image, $\Omega(x)$ is the square window centered at x, $\min_{c\in\{\text{R,G,B}\}}(\cdot)$ is the smallest of three channels of the image, and $\min_{y\in\Omega(x)}(\cdot)$ is the minimum value filtering function with the window centered at x.

By applying the minimum value filtering function to both sides of Eq. (1) and dividing it by A^c, we can get

$$\min_{y\in\Omega(x)}\left(\min_{c\in\{\text{R,G,B}\}}\left(\frac{I^c(y)}{A_c}\right)\right)=$$

$$t(x)\min_{y\in\Omega(x)}\left(\min_{c\in\{\text{R,G,B}\}}\left(\frac{J^c(y)}{A^c}\right)\right)+1-t(x). \tag{2}$$

By substituting Eq. (1) into Eq. (2), we get the transmission rate described as

$$t(x)=1-\min_{y\in\Omega(x)}\left(\min_{c\in\{\text{R,G,B}\}}I^c(y)/A^c\right). \tag{3}$$

By substituting $t^c(x)$ and A_c into optical imaging model $I^c(x)=J^c(x)t^c(x)+A^c(1-t^c(x))$, original scene image is restored after defogging by

$$J^c(x)=A^c+\frac{I^c(x)-A_c}{t^c(x)}. \tag{4}$$

2 Proposed method

Here, we propose a color, detail, contrast, and mulit-scale fusion (CDCM) algorithm. It consists of four parts: color restoration, detail enhancement, contrast enhancement, and multi-scale fusion. The first part responses to the challenges of color cast in underwater scenes, the second part is to do detail enhancement, the third part is to improve the contrast of the image, and the last part improves the global effect of the image through multi-scale fusion. The flowchart of CDCM underwater image enhancement algorithm is depicted in Fig.1.

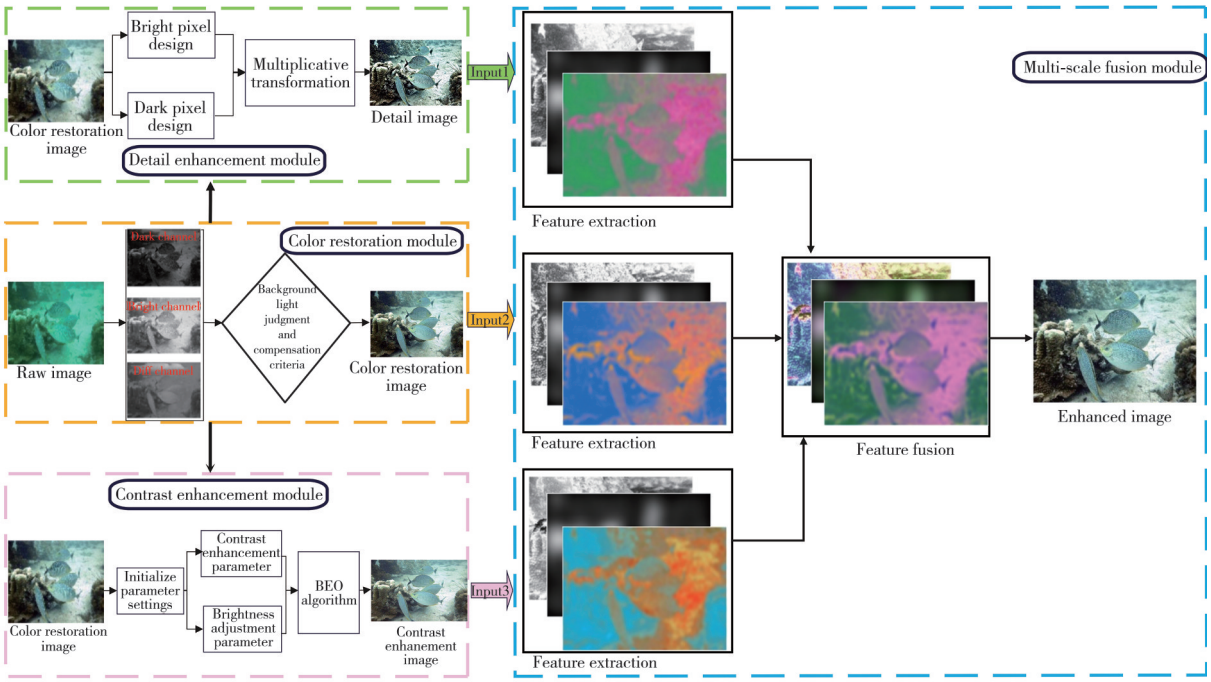

Fig. 1 Flowchart of proposed CDCM algorithm

2.1 Color restoration

Inspired by DCP algorithm, we propose a method to determine the background light of underwater images according to the difference between dark and light channels as well as channel information so as to avoid color fading of the images taken from underwater. After estimating the background light, we design adaptive color compensation strategies that take both the degree of discoloration and the attenuation level of the color channels to restore underwater images. The detailed steps are as follows:

Step 1 Computation of maximum dark-bright channel difference.

Dark channel means selecting the minimum color value of each pixel in an image block to estimate the depth information of the image. For an underwater image I, represented by its red (R), green (G), and blue (B) channels as I_{R}, I_{G}, and I_{B}, the dark channel is defined as

$$darkchannel(x,y)=\min_{(i,j)\in\Omega(x,y)}\left(\min_{c\in\{\mathrm{R,G,B}\}}(I^{c}(i,j))\right),\tag{5}$$

where $\Omega(x,y)$ denotes a local patch centered at pixel location (x,y). In practice, for typical underwater images, the red channel often dominates the dark channel, as illustrated in Fig.2 (a).

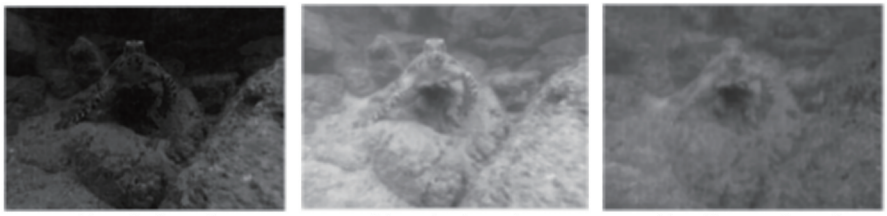

(a) Dark channel (b) Bright channel (c) Difference channel

Fig. 2 Schematic diagram of dark, bright, and difference channels

The bright channel is constructed by taking the maximum intensity value between the blue and green channels within the same local patch, as shown in Fig.2 (b).

$$brightchannel(x,y)=\max_{(i,j)\in\Omega(x,y)}\left(\max\left(I_{\mathrm{B}}(i,j),I_{\mathrm{G}}(i,j)\right)\right).\tag{6}$$

The difference channel is then computed as the absolute difference between the dark and bright channels, as shown in Fig.2 (c).

$$diffchannel(x,y)=\left|darkchannel(x,y)-brightchannel(x,y)\right|.\tag{7}$$

Finally, the color cast is assessed by identifying the pixel location $(x_{\max},y_{\max})$ where the difference channel attains its maximum value. At this location, the original pixel values from image I are extracted: $r=I_{\mathrm{R}}(x,y)$, $g=I_{\mathrm{G}}(x,y)$, and $b=I_{\mathrm{B}}(x,y)$.

Step 2 Determination of background light type

The type of background lights of marine life is gauged by the difference between the blue and green pixel values and the difference between the red and blue pixel values. The specific criteria are as follows:

If $b-g>0.05$, background light is classified as blue;

If $g-b>0.05$ and $r-b\leqslant 0.05$, background light is classified as green;

If $g-b>0.05$ and $r-b>0.05$, background light is classified as yellow;

Otherwise, underwater image I is considered free of color cast.

The threshold of 0.05 is set based on a large number of image experiments and observation results.

Step 3 Color compensation

Based on the identified background light type, R, G, B channels are compensated accordingly to obtain the color-restored image I_{CR}, as is illustrated in Fig. 4 (b). The compensation strategies are detailed below:

1) Blue background light

Red and green channels are compensated using the compensation factor α, and adjusted according to the mean values of the blue channel (μ_{B}), red channel (μ_{R}), and green channel (μ_{G}) to be as

$$\begin{cases}I'_{\mathrm{R}}=I_{\mathrm{R}}+\xi(\mu_{\mathrm{B}}-\mu_{\mathrm{R}})(1-I_{\mathrm{R}})I_{\mathrm{G}},\\ I'_{\mathrm{G}}=I_{\mathrm{G}}+\xi(\mu_{B}-\mu_{G})(1-I_{G})I_{B},\\ I'_{\mathrm{B}}=I_{\mathrm{B}},\end{cases}\tag{8}$$

where ξ is the compensation coefficient (typically $\xi=1$), controlling compensation intensity.

2) Green background light

No compensation for green channel, while red and blue channels are adjusted based on the mean value of green channel to be as

$$\begin{cases}I'_{\mathrm{R}}=I_{\mathrm{R}}+\xi(\mu_{\mathrm{G}}-\mu_{\mathrm{R}})(1-I_{\mathrm{R}})I_{\mathrm{G}},\\ I'_{\mathrm{G}}=I_{\mathrm{G}},\\ I'_{\mathrm{B}}=I_{\mathrm{B}}+\xi(\mu_{\mathrm{G}}-\mu_{\mathrm{B}})(1-I_{\mathrm{B}})I_{\mathrm{G}},\end{cases}\tag{9}$$

3) Yellow background light

Red and green channels are preserved, and only blue channel is compensated to be as

$$\begin{cases} I'_{\mathrm{R}} = I_{\mathrm{R}}, \\ I'_{\mathrm{G}} = I_{\mathrm{G}}, \\ I'_{\mathrm{B}} = I_{\mathrm{B}} + \xi(\mu_{\mathrm{G}} - \mu_{\mathrm{B}})(1 - I_{\mathrm{B}})I_{\mathrm{G}}. \end{cases} \tag{10}$$

4) No significant color cast

If the image exhibits no noticeable color cast, no compensation is performed as

$$I'_{\mathrm{R}} = I_{\mathrm{R}},\ I'_{\mathrm{G}} = I_{\mathrm{G}},\ I'_{\mathrm{B}} = I_{\mathrm{B}}. \tag{11}$$

Fig.3 displays the histogram distributions of underwater images with different color cast types before and after color restoration. It can be seen from Fig.3 that the recommended color restoration scheme effectively compensates for attenuated channels, thereby achieving color correction of underwater images. This method demonstrates robust applicability across diverse underwater color-cast scenarios.

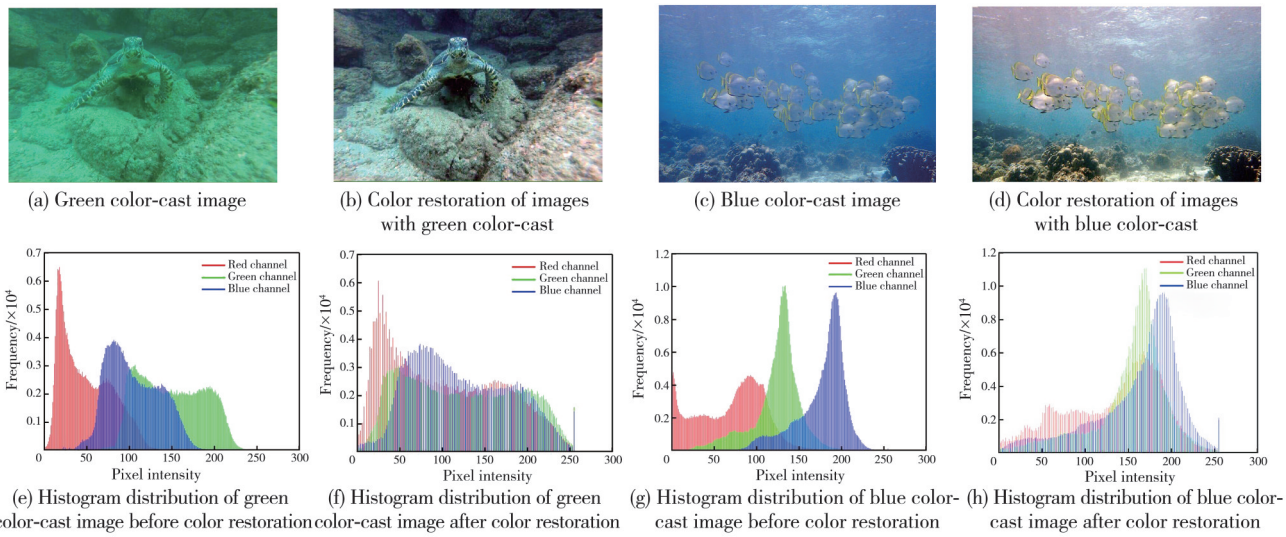

(a) Green color-cast image (b) Color restoration of images with green color-cast (c) Blue color-cast image (d) Color restoration of images with blue color-cast

(e) Histogram distribution of green color-cast image before color restoration (f) Histogram distribution of green color-cast image after color restoration (g) Histogram distribution of blue color-cast image before color restoration (h) Histogram distribution of blue color-cast image after color restoration

Fig. 3 Underwater images with different color cast types and their histogram distributions before and after color restoration

2.2 Detail enhancement

Although color restoration addresses color distortion of underwater images, loss of light often causes loss of fine details. Accordingly, we employ morphological transformation[31] to recover detailed information. Morphological transformation enhances image details through such operations as dilation and erosion using structuring elements.

The dilation and erosion operators in terms of morphological transformation are set as $G \oplus B$ and $G \ominus B$, respectively, where G is the input image and B is the structuring element.

$$G \oplus B = \bigcup G_{b,B},\ G \ominus B = \bigcup G_{-b,B}, \tag{12}$$

where G_b denotes the basic shift operation of B in the b-direction, and $G_{-b,B}$ represents the basic shift operation of B in the opposite direction of the b direction.

The closing and opening operators of morphological transformation are defined as $G \bullet B$ and $G \circ B$, respectively.

$$G \bullet B = (G \oplus B) \ominus B,\ G \circ B = (G \ominus B) \oplus B, \tag{13}$$

The white top-hat ($\boldsymbol{Q}$) and black top-hat ($\boldsymbol{R}$) operators are further defined as

$$Q = G - G \circ B,\ R = G \bullet B - G. \tag{14}$$

To enhance image details, two distinct components are designed: brightness enhancement component ($\boldsymbol{Q}_{\mathrm{w}}$) and darkness enhancement component ($\boldsymbol{R}_{\mathrm{b}}$). The former enhances foreground brightness by increasing the luminance of target regions relative to their surroundings, and the latter strengthens background dark pixels by boosting the luminance of dark regions, that is

$$\begin{cases} \boldsymbol{Q}_{\mathrm{w}}(I_{\mathrm{CR}}, B_1, B_2) = I_{\mathrm{CR}} - (I_{\mathrm{CR}} \circ B_1) \bullet B_2 \\ \boldsymbol{R}_{\mathrm{b}}(I_{\mathrm{CR}}, B_1, B_2) = (I_{\mathrm{CR}} \bullet B_1) \circ B_2 - I_{\mathrm{CR}} \end{cases}, \tag{15}$$

where B_1 and B_2 are square-shaped structuring elements with sizes of 15×15 and 5×5, respectively.

After extracting the bright and dark pixel regions from the image, image enhancement is achieved by subtracting the bright pixel regions from the dark pixel regions. To further accentuate the contours of foreground objects and improve their separation from the background, the resulting image undergoes n power-law operations, ultimately yielding the detail-enhanced image $\boldsymbol{I}_{\mathrm{DE}}$, as shown in Fig.4(c). Thus, the proposed model successfully enhances the visibility and clearness of the underwater image.

$$\boldsymbol{I}_{\mathrm{DE}} = \boldsymbol{I}_{\mathrm{CR}} + \omega \sum_{i=1}^{n} (\boldsymbol{Q}_{\mathrm{w}}(I'_1, B_1, B_2) - \boldsymbol{R}_{\mathrm{b}}(I'_1, B_1, B_2)), \tag{16}$$

where n denotes the iteration count, set to 10, to prevent over-enhancement and distortion, and ω is the enhancement factor, set to 0.1.

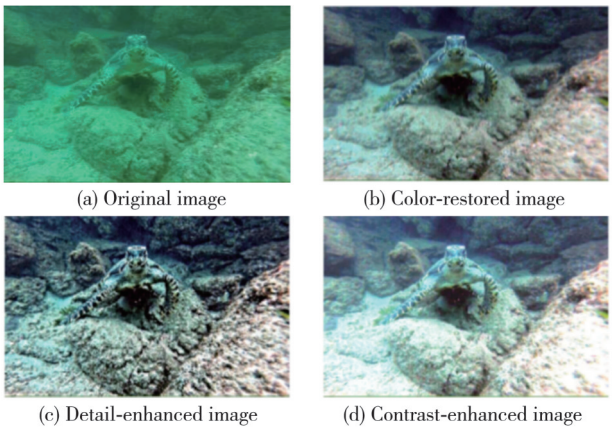

Fig. 4 Enhanced images at different stages

2.3 Contrast enhancement

In the previous sections, color restoration and detail enhancement have achieved the restoration of color distortion and the enhancement of blurred details of underwater images.

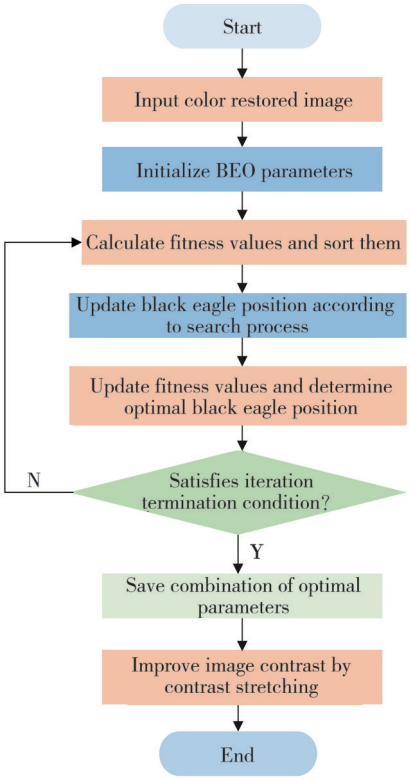

Fig. 5 Flowchart of BEO contrast enhancement algorithm

However, the problem of low contrast still exists and requires further improvement. To avoid loss of details or noise amplification during contrast enhancement, for the underwater images after color restoration, we use BEO[30] based contrast enhancement method (its flowchart can be seen in Fig. 5) to optimize the contrast enhancement coefficient and the brightness adjustment coefficient by simulating the search process of BEO algorithm, and consequently, the detail clarity and color reproduction of the image are significantly improved. Through continuous iterative optimization, the final enhanced image, as seen in Fig.4(d), demonstrates excellent performance in contrast enhancement.

Step 1 Parameter settings and initialization

The total number of eagles n_{eagles} was set to 30, the maximum iterations $n_{\text{max,iter}}$ was set to 100, and the position of each eagle individual was initialized.

To demonstrate the robustness of the proposed method and ensure it is not over-optimized for specific images, a sensitivity analysis was conducted in terms of key parameters: eagle population size (n_{eagles}) and maximum iterations ($n_{\text{max,iter}}$). The analysis was performed on a diverse underwater image dataset, and the performance was evaluated using quality index: fitness function. We randomly selected 10 underwater images to calculate the quality indexes for different numbers of black eagles and iterations, and the mean values and standard deviations of the results are shown in Tables 1 and 2.

Table 1 Sensitivity of the number of eagles to quality indexes at $n_{\text{max,iter}}$=100

n_{eagles}	Mean value	Standard deviation
20	0.479 5	0.129 7
25	0.506 9	0.162 3
30	0.542 3	0.122 6
35	0.546 4	0.128 7
40	0.531 6	0.151 1

Table 2 Sensitivity of the maximum iterations to quality indexes at n_{eagles}=30

$n_{\text{max,iter}}$	Mean value	Standard deviation
50	0.480 2	0.142 7
75	0.494 1	0.156 6
100	0.524 8	0.130 0
125	0.519 0	0.163 0
150	0.499 7	0.129 0

We conducted an experiment on the influence of the number of black eagles n_{eagles} on the quality indexes when the number of iterations was 100. As shown in Table 1, when $n_{\text{eagles}}=30$, although the mean value is not the highest, the standard deviation is the smallest and the robustness is the best. Therefore, we chose $n_{\text{eagles}}=30$ instead of 35. To further verify the stability of the experimental parameters on the results, we conducted an experiment on the influence of iterations on the quality indexes at $n_{\text{eagles}}=30$. As shown in Table 2, when $n_{\text{max,iter}}$ is 100, the mean value is the best and the standard deviation is also the smallest. Therefore, we selected the iterations as 100. Each individual's position is composed of six parameters: $h_{\text{CE}}(r)$, $h_{\text{CE}}(g)$, $h_{\text{CE}}(b)$, $l_{\text{BR}}(r)$, $l_{\text{BR}}(g)$, and $l_{\text{BR}}(b)$, where the first three parameters represent the contrast enhancement coefficients for the

R, G, B channels respectively, and the last three parameters represent the brightness adjustment coefficients for the R, G, B channels respectively. The positions of the eagle individuals are initialized to random values between 0.5 and 1 by

$$p_{\text{eagle}}(i,:)=0.5+0.5\times\text{rand}(1,6), \tag{17}$$

where $p_{\text{eagle}}(i,:)$ indicates the position of the ith eagle.

Step 2 Definition of fitness function

To evaluate the image's contrast enhancement effect, the image's standard deviation (std2)[32], entropy[32], and Sobel edge strength[32] are comprehensively considered. We define a fitness function as

$$f_{\text{fit}}=\sqrt[3]{\boldsymbol{S}_{\text{td}}(I_{\text{CR}})\times\boldsymbol{E}_{\text{n}}(I_{\text{CR}})\times\boldsymbol{S}_{\text{ob}}(I_{\text{CR}})}. \tag{18}$$

The purpose of this fitness function is to optimize the image's contrast enhancement effect by maximizing the image's contrast, detail retention, and edge clarity.

The fitness function designed is based on the following objective optimization ideas: $\boldsymbol{S}_{\text{td}}(I_{\text{CR}})$ emphasizes the contrast of the image, $\boldsymbol{E}_{\text{n}}(I_{\text{CR}})$ measures the richness of information and the degree of detail preservation of the image, and $\boldsymbol{S}_{\text{ob}}(I_{\text{CR}})$ evaluates the edge clarity and structural preservation ability of the image.

Step 3 BEO iteration process

In each iteration, BEO updates the position of each eagle by simulating the search process of the eagle swarm. Each update involves random changes in the eagle's position, ensuring that each position's values remain within a reasonable range of [0.1, 1.5]. During the search process, the algorithm allows parameters to descend to as low as 0.1 in order to enhance the flexibility and global search capability of the optimization process, thereby avoiding premature convergence to a local optimum.

$$\begin{cases} p_{\text{eagle}}(i,:)=p_{\text{eagle}}(i,:)+\text{rand}(1,6)\times 0.05, \\ p_{\text{eagle}}(i,:)=\max(0.1,\min(1.5,p_{\text{eagle}}(i,:))). \end{cases} \tag{19}$$

Based on the parameters of each eagle, an image enhancement effect is generated, and the contrast and brightness of all R, G, B channels are adjusted using a contrast stretching method[33] as

$$f_{\text{enhance}}(I_{\text{CR}}(c))=l_{\text{BR}}(c)+\frac{(I_{\text{CR}}(c)-l_{\text{CE}}(s))(h_{\text{BR}}(c)-l_{\text{BR}}(c))}{h_{\text{CE}}(c)-l_{\text{CE}}(c)}, \tag{20}$$

where $l_{\text{CE}}(c)$ and $h_{\text{CE}}(c)$ determine the grayscale value range of the input image, affecting the contrast, with $l_{\text{CE}}(c)=0$, $h_{\text{CE}}(c)=\min(p_{\text{eagle}}(i,c),1)$, and $c=1,2,3$, representing the R, G, and B channels respectively; $l_{\text{BR}}(c)$ and $h_{\text{BR}}(c)$ determine the grayscale intensity range of the output image, affecting the brightness adjustment, with $l_{\text{BR}}(c)=\max(p_{\text{eagle}}(i,c+3),0)$, $h_{\text{BR}}(c)=1$, and $c=1,2,3$.

Step 4 Updating the optimal solution

For each updated enhanced image, its fitness value is calculated and compared with the current best fitness value. If the current enhanced image has a better fitness value, i.e., $f_{\text{fit,curr}}>f_{\text{fit,best}}$, the optimal position and its corresponding enhancement parameters are updated, i.e., $p_{\text{eagle,best}}=p_{\text{eagle}}(i,:)$. Otherwise, they are keep unchanged. Fig.6 shows the contrast enhancement effect after every 20 iterations, with the fitness function values at 20 iterations being 0.764, at 40 iterations being 0.879, at 60 iterations being 0.879, at 80 iterations being 0.884, and at 100 iterations being 0.884, respectively.

Step 5 Getting a contrast enhanced image

After several iterations for optimization, the final enhanced image I_{CE} is calculated based on the parameters of optimal BEO algorithm.

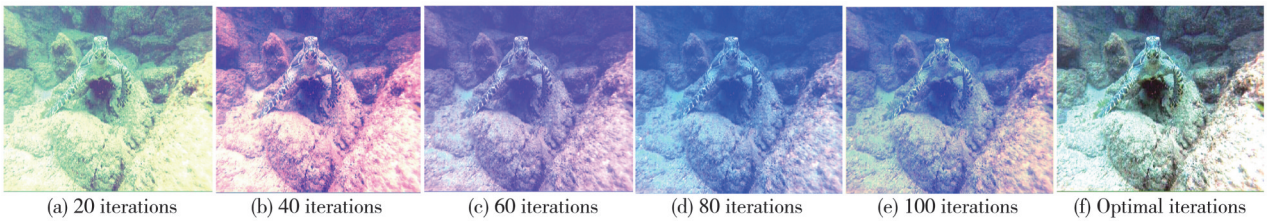

(a) 20 iterations (b) 40 iterations (c) 60 iterations (d) 80 iterations (e) 100 iterations (f) Optimal iterations

Fig. 6 Image contrast enhancement by iterative optimization algorithm

2.4 Multi-scale fusion

Color restoration helps address color distortion of underwater images, detail enhancement mitigates blurred details, and contrast improvement enhances image brightness. For underwater images with varying characteristics, we will employ a fusion method combining principal component weight[34], saliency weight, and exposure weight to enhance underwater images. The detailed arrangements consist of the following steps:

Step 1 Principal component weight extraction

In principal component analysis (PCA), an orthogonal transformation is performed to eliminate the correlation between original variables. Linearly correlated variables are projected into PCA space using the covariance matrix eigenvectors.

1) Image vectorization

Supposing that there is a gray-scale image with the size of $m \times p$, it is flattened into a column vector with the size of $mp \times 1$. Let the ith image vector be

$$\boldsymbol{X}_i = \begin{bmatrix} \boldsymbol{x}_{i,1} & \boldsymbol{x}_{i,2} & \cdots & \boldsymbol{x}_{i,mp} \end{bmatrix}^{\mathrm{T}}, \ i = 1,2,3. \quad (21)$$

2) Construction of data matrix

By concatenating the column vectors of the image, we obtain a data matrix as

$$\boldsymbol{X} = \begin{bmatrix} \boldsymbol{X}_1, \boldsymbol{X}_2, \boldsymbol{X}_3 \end{bmatrix} = \begin{bmatrix} \boldsymbol{x}_{1,1} & \boldsymbol{x}_{2,1} & \boldsymbol{x}_{3,1} \\ \boldsymbol{x}_{1,2} & \boldsymbol{x}_{2,2} & \boldsymbol{x}_{3,2} \\ \vdots & \vdots & \vdots \\ \boldsymbol{x}_{1,mp} & \boldsymbol{x}_{2,mp} & \boldsymbol{x}_{3,mp} \end{bmatrix}, \quad (22)$$

where data matrix $\boldsymbol{X}$ has the size of $mp \times 3$, each column represents a sample observation X_i, and each row represents a variable (pixel position).

3) Computation of observation scores via PCA

First, we calculate the covariance matrix by

$$\boldsymbol{C}_i = \frac{1}{mp-1} \boldsymbol{X}_i \boldsymbol{X}_i^{\mathrm{T}}, \quad (23)$$

where the size of $\boldsymbol{C}_i$ is $mp \times mp$.

Next, we solve the eigenvalues and eigenvectors of covariance matrix $\boldsymbol{C}_i$ by

$$\boldsymbol{C}_i \boldsymbol{v}_i = \lambda_i \boldsymbol{v}_i, \quad (24)$$

where λ_i is the ith eigenvalue (sorted in descending order), and $\boldsymbol{v}_i$ is the corresponding feature vector (column vector).

Afterwards, we select the eigenvectors corresponding to the top k' largest eigenvalues to construct the eigenvector matrix as

$$\boldsymbol{V}_i = \begin{bmatrix} \boldsymbol{v}_1 & \boldsymbol{v}_2 & \cdots & \boldsymbol{v}_{k'} \end{bmatrix}, \quad (25)$$

where the size of $\boldsymbol{V}_i$ is $mp \times k'$, and each column represents a principal component direction.

Finally, we get the PCA score matrix as

$$\boldsymbol{S}_i = \boldsymbol{V}_i^{\mathrm{T}} \boldsymbol{X}_i \quad (26)$$

where the size of $\boldsymbol{S}_i$ is $k' \times 1$, each row represents the projection of a principal component onto all observations, and each column represents the score of an observation across all principal components.

4) Linear normalization and reshaping

Since each row of score matrix $\boldsymbol{S}_i$ corresponds to a principal component, and each column corresponds to a sample, it can be rewritten as $\boldsymbol{S}_i = \begin{bmatrix} s_{i,1} \\ s_{i,2} \\ \vdots \\ s_{i,k'} \end{bmatrix}$.

Then, performing linear normalization on each score vector $\boldsymbol{S}_i$, we can get

$$\boldsymbol{S}_i' = \begin{bmatrix} s_{i,1}' \\ s_{i,2}' \\ \vdots \\ s_{i,k'}' \end{bmatrix}, \quad (27)$$

where $s_{i,j}' = \dfrac{s_{i,j} - \min(s_{i,j})}{\max(s_{i,j}) - \min(s_{i,j})}$.

Finally, applying a simple Gaussian smoothing filter $\boldsymbol{G}_{\mathrm{f}}$ to $\boldsymbol{S}_i'$, we can get

$$\boldsymbol{X}_i' = \boldsymbol{G}_{\mathrm{f}} \otimes \boldsymbol{S}_i', \quad (28)$$

where $\boldsymbol{X}_i'$ is the $m \times p$ smoothed matrix, and $\otimes$ represents convolution operation.

The PCA weight map $\boldsymbol{W}_{\mathrm{PCA},i}(r,c)$ corresponding to $\boldsymbol{X}_i$ is expressed as

$$\boldsymbol{W}_{\mathrm{PCA},i}(r,c) = \frac{\boldsymbol{X}_i'(r,c)}{\sum_{r=1}^{m}\sum_{c=1}^{p} \boldsymbol{X}_i'(r,c)}, \ (i = 1,2,3). \quad (29)$$

Let $\boldsymbol{W}_{\mathrm{PCA},k} = \boldsymbol{W}_{\mathrm{PCA},i}$, $\boldsymbol{W}_{\mathrm{PCA},k}$ represents the principal component weight of I_{CR}, I_{DE}, and I_{CE}.

Step 2 Saliency weight extraction

The Saliency weight $W_{\mathrm{SAL},k}$ aims to reinforce the contrast between the light and dark areas, hence improving overall image contrast and making less conspicuous objects in underwater environments more prominent[35].

$$\boldsymbol{W}_{\mathrm{SAL},k} = (L_k - \overline{L_k})^2 - (A_k - \overline{A_k})^2 + (B_k - \overline{B_k})^2, \quad (30)$$

where subscript k refers to the three image processing methods mentioned earlier, namely CR, DE, and CE; L_k represents the pixel value of the luminance channel by using k method; A_k and B_k represent the pixel values of the two color channels by using k method; $\overline{L_k}$, $\overline{A_k}$, and $\overline{B_k}$ are the average pixel values of the three channels by using k method, respectively; and $\boldsymbol{W}_{\mathrm{SAL},k}$ represents the significance weight of I_{CR}, I_{DE} and I_{CE}.

Step 3 Exposure weight extraction

The exposure weight $\boldsymbol{W}_{\mathrm{EXP},k}$ enhances the contribution of highly visible regions in the fused image by optimizing exposure levels using k method to ensure rich tonal gradations across all pixels. A higher $\boldsymbol{W}_{\mathrm{EXP},k}$ indicates better exposure balance and improved visibility in the corresponding region.

$$\boldsymbol{W}_{\mathrm{EXP},k} = \exp\left(-\frac{(L_k - 0.5)^2}{2 \times 0.25^2}\right). \quad (31)$$

Step 4 Weight normalization

After computing the three weight maps, their combined weight W_k is calculated as

$$\boldsymbol{W}_k = \boldsymbol{W}_{\mathrm{PCA},k} + \boldsymbol{W}_{\mathrm{SAL},k} + \boldsymbol{W}_{\mathrm{EXP},k}. \quad (32)$$

Subsequently, W_k is normalized to ensure a total weight sum of 1 as

$$\overline{\boldsymbol{W}_k} = \frac{\boldsymbol{W}_k}{\boldsymbol{W}_{\mathrm{CR}} + \boldsymbol{W}_{\mathrm{DE}} + \boldsymbol{W}_{\mathrm{CE}}}, \quad (33)$$

where $\boldsymbol{W}_{\mathrm{CR}}$ is the sum of $\boldsymbol{W}_{\mathrm{PCA,CR}}$, $\boldsymbol{W}_{\mathrm{SAL,CR}}$ and $\boldsymbol{W}_{\mathrm{EXP,CR}}$. Similarly, $\boldsymbol{W}_{\mathrm{DE}}$ and $\boldsymbol{W}_{\mathrm{CE}}$ are computed analogously to

$\boldsymbol{W}_{\mathrm{CR}}$. Each $\overline{\boldsymbol{W}_k}$ represents the weight map of the input image by using k method and serves as the fusion weight.

Step 5 Multi-scale pyramid fusion

After applying Gaussian blur and down sampling to the weight maps and input images to construct a Gaussian pyramid with l layers (l represents the number of decomposition layers of the pyramid), we obtain the final fused image through an image reconstruction step as

$$L\{F^l\}=\sum_{l=1}^{N}G_{\mathrm{p}}\{\boldsymbol{W}_k^l\}\times L\{I_k^l\}, \tag{34}$$

where G_{p} denotes Gaussian pyramid decomposition, L denotes Laplacian pyramid decomposition, $L\{I_k^l\}$ is the Laplacian map of the input component I_k^l, $G_{\mathrm{p}}\{\boldsymbol{W}_k^l\}$ is the Gaussian weight map of the normalized weight $\overline{\boldsymbol{W}_k}$.

Finally, by upsampling the output image pyramid, we obtain the new combined image as

$$I_{\mathrm{final}}=\sum_{l=1}^{3}L\{F^l\}. \tag{35}$$

The results of weight extraction and the enhanced output image are illustrated in Fig.7.

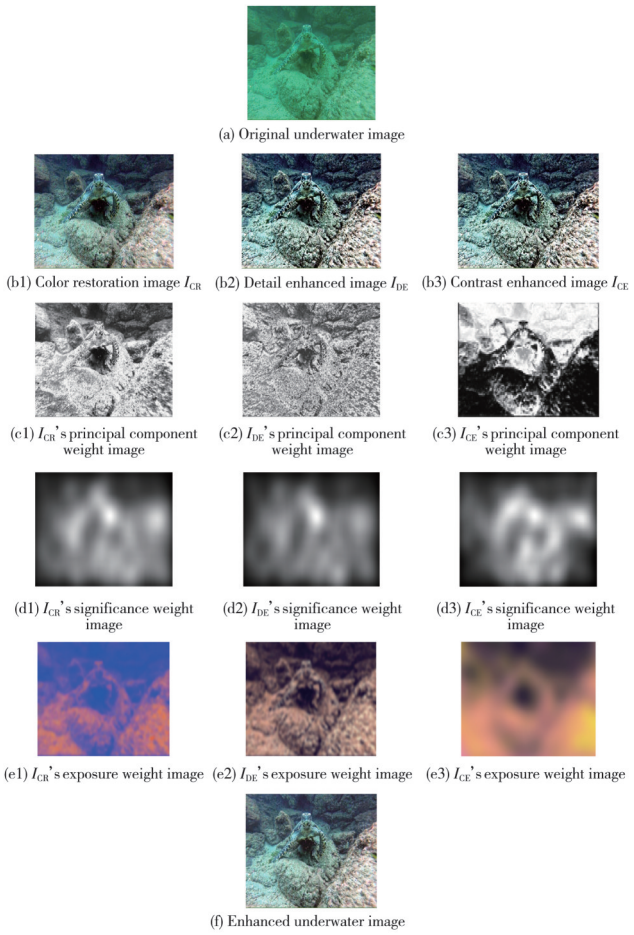

Fig. 7 Extracting weight images from three images b1, b2, and b3, and performing image fusion

Algorithm 1 describes the proposed algorithm.

Algorithm 1: CDCM algorithm

Input Underwater degradation image I

1: Decompose R, G and B channels of input image I
2: $darkChannel \leftarrow I_{\mathrm{R}}$, $brightChannel \leftarrow \max(I_{\mathrm{B}}, I_{\mathrm{G}})$
3: $diffChannel \leftarrow |I_{\mathrm{R}} - \max(I_{\mathrm{B}}, I_{\mathrm{G}})|$
4: Determine the location (x, y) of the maximum value in difference channel and pixel values r, g, b
5: if $b - g > 0.05$
6: Using Eq.(8) for compensating the channel, color restoration image I_{CR} is obtained.
7: else if $g - b > 0.05$ and $r - b \leqslant 0.05$
8: Using Eq.(9) for compensating the channel, color restoration image I_{CR} is obtained.
9: else if $g - b > 0.05$ and $r - b > 0.05$
10: Using Eq.(10) for compensating the channel, color restoration image I_{CR} is obtained.
11: else
12: Using Eq.(11) for compensating the channel, color restoration image I_{CR} is obtained.
13: end
14: Bright pixel $\leftarrow Q_{\mathrm{w}}(I_{\mathrm{CR}}, B_1, B_2) = I_{\mathrm{CR}} - (I_{\mathrm{CR}} \circ B_1) \cdot B_2$
Dark pixel $\leftarrow R_{\mathrm{b}}(I_{\mathrm{CR}}, B_1, B_2) = (I_{\mathrm{CR}} \cdot B_1) \circ B_2 - I_{\mathrm{CR}}$
15: According to Eq.(16), I_{CR} is enhanced to obtain detail enhanced image I_{DE}.
16: According to Eqs.(17)–(20), the contrast of I_{CR} is improved based on the BEO algorithm, and the contrast enhanced image I_{CE} is obtained
17: According to Eqs.(21)–(35), multi-scale fusion of I_{CR}, I_{DE}, and I_{CE} is carried out to obtain fused image I_{final}.

Output Underwater enhanced image I_{final}

3 Experimental results and analysis

This section evaluates the validity of the proposed algorithm through qualitative and quantitative analyses, alongside subjective and objective evaluations. We demonstrate the robustness and efficacy of our method in addressing common underwater imaging problems in diverse scenarios. The experiments were conducted on two datasets: UIEB [25] and RUIE[36].

3.1 Color restoration experiment

To validate the accuracy of designed color restoration module, we tested it against three established color correction methods: gray world (GW) [37], white patch (WP) [38], and adaptive white balance (AWB) [39]. The experiments were conducted on RUIE dataset, with the results illustrated in Fig.8.

It can be seen from Fig.8(b) that the GW method exhibits excessive compensation in the red channel when processing blue- or green-dominated images, resulting in prominent red artifacts. The WP approach fails to adequately correct color casts, as shown in Fig.8(c), where residual color distortion and a hazy layer persist. While both AWB method and our method demonstrate effective color cast correction. A comparison between Fig.8(d) and Fig.8(e) reveals that AWB method introduces overexposure and residual red artifacts.

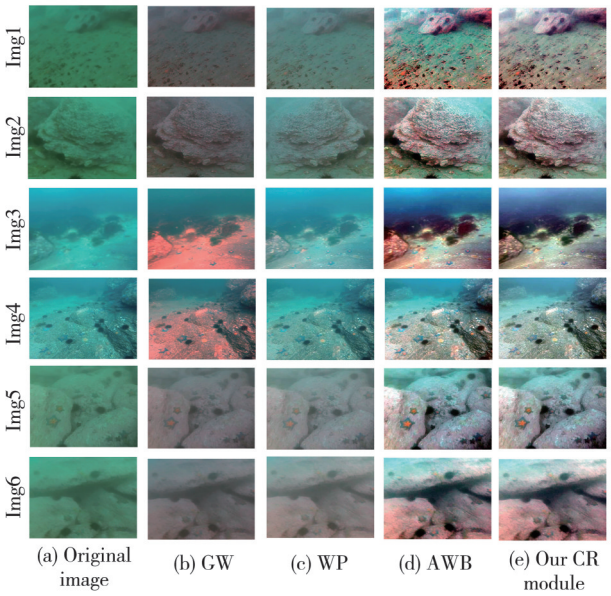

Fig. 8 Comparison of different color restoration methods

The experimental results confirm that our CR module accurately estimates the background light of underwater images and applies channel-specific compensation tailored to different color casts. This approach maximizes the recovery of colors.

3.2 Subjective analysis

Underwater images with varying levels of degradation from the UIEB and RUIE datasets are selected to assess the applicability and robustness of the proposed method. The comparative methods include UDCP[12], IBLA[4], ACCC[22], HFM[21], CCWD[20], CCRA[19], Water-Net[25], UWCNN-SD[26], and our method.

Fig. 9 illustrates the enhancement results of different algorithms applied to randomly extracted underwater images from UIEB dataset. It can be observed that, from an overall visual perspective, UDCP and IBLA algorithms improve image contrast to some extent but fail to effectively correct severe color casts.

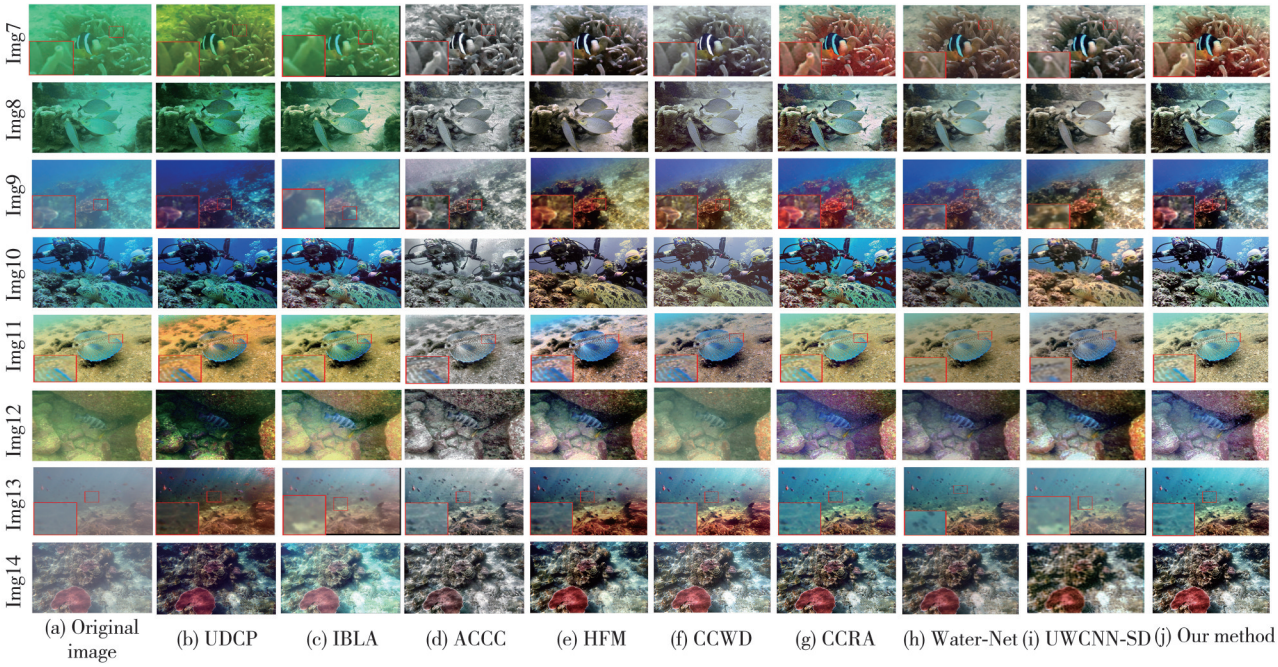

Fig. 9 Comparison of different methods on UIEB dataset

ACCC algorithm producs images with insufficient color saturation, resulting in an overall grayish appearance. Both HFM and CCRA algorithms introduce varying degrees of red artifacts during color compensation, indicating over-compensation. Although CCWD algorithm effectively addresses color cast problem, it sufferes from detail blurring in certain regions. Water-Net and UWCNNSD algorithms preserve image textures well, but the former exhibites low contrast, while the latter shows noticeable over-enhancement. In terms of image details, by examining the locally magnified areas within red dashed boxes in Fig. 9(i), it can be more clearly observed that compared to IBLA algorithm that achieves the highest contrast and UWCNN-SD algorithm that preserves the sharpest details, our proposed algorithm successfully suppresses over-enhancement while restoring more natural colors. Moreover, its detail richness is comparable to that of UWCNN-SD and significantly superior to that of IBLA. Compared to CCWD algorithm, which also emphasizes color and detail preservation, our method shows no detail loss in the locally magnified regions and maintains more complete structural integrity.

Fig. 10 displays the enhancement results of various algorithms applied to randomly selected underwater images from RUIE dataset. In terms of color restoration, although UDCP and IBLA algorithms enhance the details, they have serious color distortion. ACCC algorithm completely loses color information and outputs gray images. Both HFM and CCRA algorithms fail to accurately balance the color. The former is blurred in detail, while the latter introduces serious red artifacts and excessive enhancement when processing green color-cast images. In terms of detail and contrast, although CCWD algorithm has good basic contrast and detail, the image as a whole is disturbed by fog effect. The color retention of Water-Net algorithm is acceptable, but the detail enhancement is obviously insufficient. UWCNN-SD algorithm performs well in detail recovery and color deviation correction, but there still exists room for improvement of overall contrast. In contrast, our algorithm shows significant advantages in local enlarged regions. The color restoration is the most natural, effectively avoiding the red artifacts of CCRA and the graying of ACCC. The richness of details is similar to that of UWCNN-SD, and is significantly better than that of Water-Net and HFM. At the same time, its contrast is properly controlled, eliminating the fog of CCWD.

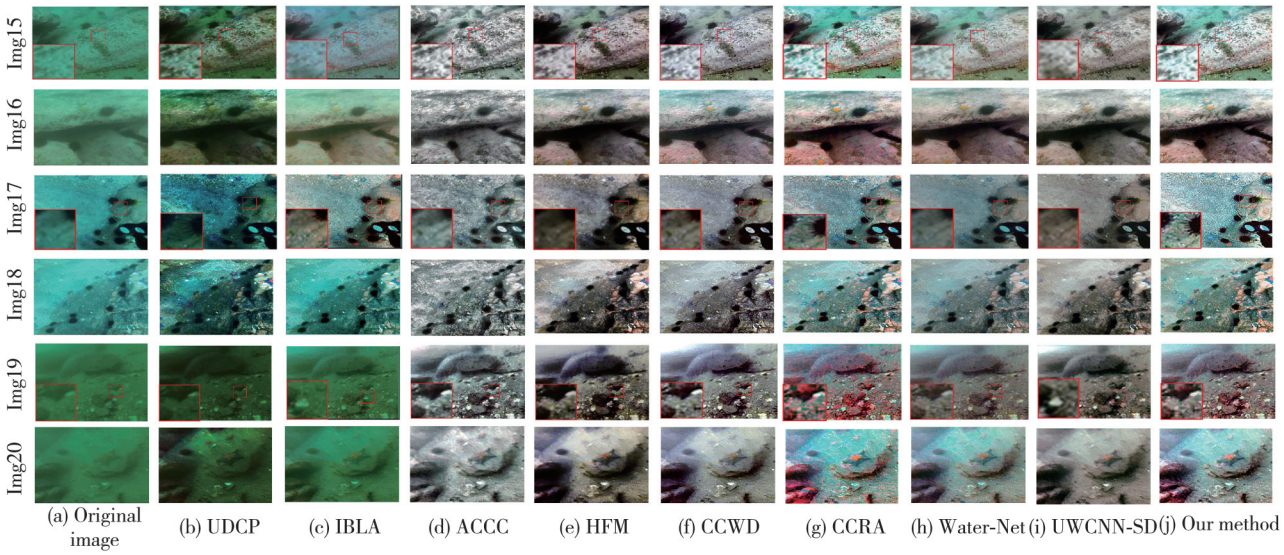

Fig. 10 Comparison of different methods on RUIE dataset

Relatively speaking, our algorithm achieves the best visual balance in overall color naturalness, contrast, and local detail preservation. More details can be seen from the enlarged images in Fig.11.

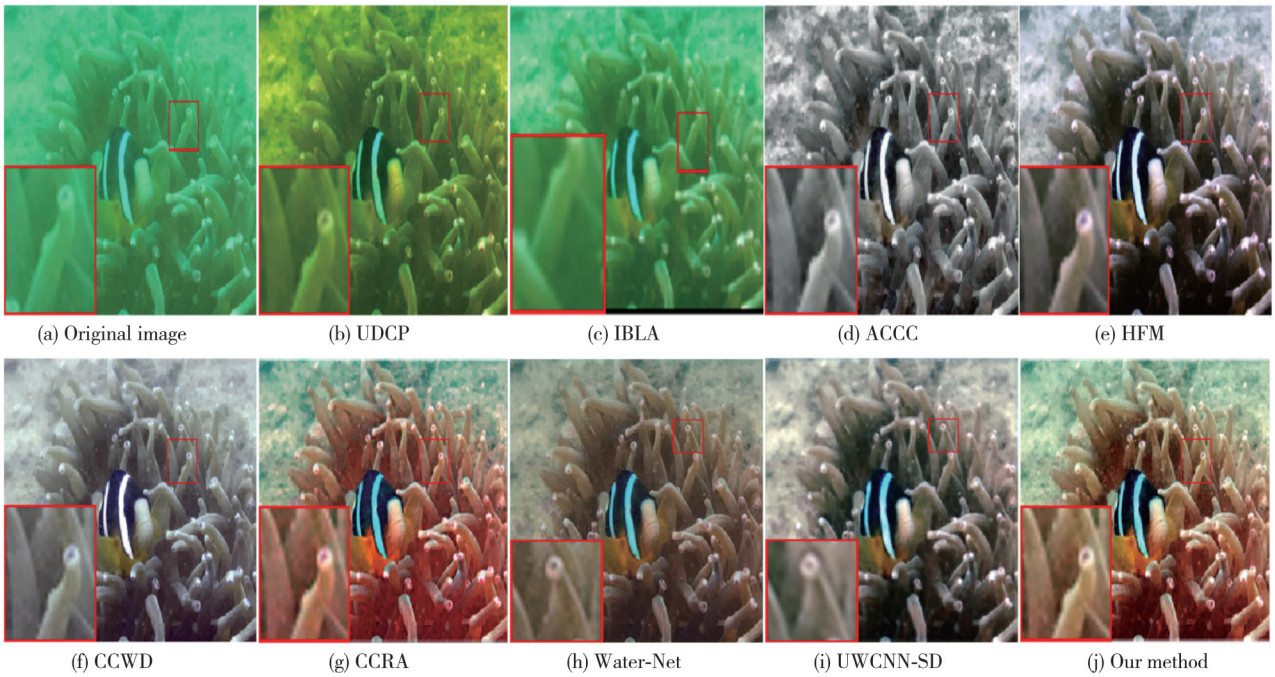

Fig. 11 Comparison of partial enlarged images

3.3 Objective analysis

To mitigate potential human bias in subjective analysis, we additionally selected two no-reference metrics: UCIQE[40] and UIQM[41], as well as three full-reference metrics: AG[42], IE[43], and PCQI[44], to fully analyze the effectiveness and robustness of our method.

Table 3 shows a comparison of different methods in terms of metrics on UIEB dataset. It can be seen that our algorithm obtains higher UCIQE and UIQM values in most cases, and individual index values are lower than those of the comparison algorithms. Moreover, its average value is the highest among the five indexes. Also, the robustness and effectiveness of our model are confirmed.

Table 3 UCIQE, UIQM, AG, IE and PCQI results on UIEB dataset

Method	Image No.	UDCP	IBLA	ACCC	HFM	CCWD	CCRA	Water-Net	UWCNN-SD	Our method
UCIQE	Img7	0.52	0.47	—	—	0.63	0.65	0.64	0.65	0.64
	Img8	0.56	0.54	—	—	0.58	0.61	0.58	0.62	0.64
	Img9	0.57	0.51	—	—	0.63	0.65	0.63	0.62	0.65
	Img10	0.61	0.68	—	—	0.62	0.70	0.64	0.62	0.65
	Img11	0.63	0.64	—	—	0.62	0.62	0.61	0.63	0.63
	Img12	0.63	0.61	—	—	0.63	0.64	0.64	0.64	0.65
	Img13	0.62	0.51	—	—	0.66	0.66	0.68	0.66	0.69
	Img14	0.62	0.57	—	—	0.64	0.65	0.64	0.64	0.66
	Mean	0.59	0.57	—	—	0.63	0.65	0.63	0.63	**0.65**
UIQM	Img7	1.67	0.15	3.68	3.31	3.26	4.99	5.56	5.19	4.16
	Img8	4.46	2.73	5.13	5.11	4.99	4.66	4.80	5.03	4.17
	Img9	2.52	1.65	4.81	4.29	4.31	4.21	4.50	4.79	5.59
	Img10	1.54	2.85	4.75	4.29	4.34	3.12	4.49	5.41	4.55
	Img11	6.04	4.40	5.54	5.07	4.94	5.09	5.24	4.80	5.16
	Img12	3.60	3.79	4.73	4.64	4.56	4.86	5.55	5.10	5.67
	Img13	4.67	3.08	4.07	3.82	3.90	2.91	4.04	5.31	5.49
	Img14	4.99	3.71	5.23	4.63	5.03	4.99	5.77	3.68	5.62
	Mean	3.69	2.80	4.74	4.39	4.42	4.35	4.99	4.91	**5.05**
AG	Img7	2.78	3.27	5.20	4.37	4.51	6.86	7.83	8.69	5.49
	Img8	9.08	10.36	15.50	11.00	10.98	17.69	10.43	8.05	15.69
	Img9	6.79	6.18	13.64	9.19	11.31	12.70	7.93	7.11	12.76
	Img10	11.76	13.94	15.08	14.02	14.31	18.39	12.54	12.41	19.69
	Img11	12.31	12.35	18.14	17.40	16.36	16.14	10.66	9.83	17.80
	Img12	2.74	3.18	5.02	3.84	4.58	5.84	7.55	6.89	4.66
	Img13	7.09	5.37	12.42	8.86	13.06	13.74	8.44	8.99	15.64
	Img14	11.73	12.55	18.79	15.99	18.44	20.98	13.98	7.11	22.39
	Mean	8.04	8.40	12.97	10.58	11.69	14.04	9.92	8.63	**14.26**
IE	Img7	3.20	5.88	11.65	4.86	10.49	7.64	8.79	6.77	8.26
	Img8	4.38	7.11	6.82	5.05	5.30	7.91	6.37	11.04	8.70
	Img9	6.84	4.78	5.49	5.78	4.96	7.68	4.31	5.35	6.76
	Img10	9.30	8.80	6.72	6.75	6.47	7.56	5.32	5.97	10.19
	Img11	16.51	0.94	20.14	12.61	17.36	7.57	16.96	9.80	18.63
	Img12	1.81	19.47	4.35	5.45	5.67	7.64	7.10	5.98	6.51
	Img13	2.85	5.93	5.62	6.95	7.93	7.70	5.57	6.17	7.37
	Img14	3.30	5.24	5.08	6.53	5.74	7.78	3.89	2.84	7.03
	Mean	6.02	7.27	8.23	6.75	7.99	7.69	7.29	6.74	**9.18**
PCQI	Img7	1.03	1.12	1.23	1.12	1.15	1.29	1.23	1.22	1.23
	Img8	0.99	1.13	1.34	1.14	1.19	1.36	1.26	1.24	1.28
	Img9	0.85	1.13	0.98	1.17	1.25	1.25	1.26	1.24	1.28
	Img10	0.90	1.07	0.79	1.09	1.00	1.16	1.10	1.12	1.16
	Img11	1.05	1.04	1.17	1.14	1.06	1.20	1.23	1.23	1.26
	Img12	0.80	1.11	1.28	1.13	1.13	1.21	1.19	1.24	1.21
	Img13	1.06	1.19	1.13	1.19	1.34	1.30	1.30	1.30	1.34
	Img14	0.94	1.17	1.16	1.18	1.30	1.24	1.15	1.00	1.29
	Mean	0.95	1.12	1.14	1.14	1.18	1.25	1.21	1.20	**1.26**

Table 4 shows a comparison of different methods in terms of metrics on RUIE dataset. Among them, our algorithm obtains the best evaluation values in AG and PCQI, UWCNN-SD algorithm obtains the best average values in UCIQE and UIQM, and Water-Net algorithm obtains the best average value of IE. Although our algorithm does not get the best average value in UCIQE, UIQM and IE, it is better than other

algorithms, which also verifies the effectiveness and robustness of our algorithm.

It can be seen from Tables 3 and 4 that UCIQE scores on UIEB dataset of our method and CCRA are both 0.65, which are the best. The UIQM performance of our method is better than that of Water-Net, with a growth of 1.20%. The AG value of our method is slightly higher than that of CCRA, increasing by 1.57% and enhancing edge and texture details. The IE value of our method is significantly better than that of CCWD, increasing by 14.89% and restoring the richness and details of the image. The PCQI value of our method has increased by 0.80% than that of CCRA, maintaining a leading position in perceived quality.

Table 4 UCIQE, UIQM, AG, IE and PCQI results on RUIE dataset

Method	Image No.	UDCP	IBLA	ACCC	HFM	CCWD	CCRA	Water-Net	UWCNN-SD	Our method
UCIQE	Img15	0.52	0.50	0.54	—	—	0.63	0.57	0.63	0.60
	Img16	0.54	0.49	0.57	—	—	0.62	0.66	0.65	0.62
	Img17	0.61	0.59	0.59	—	—	0.60	0.65	0.64	0.61
	Img18	0.59	0.55	0.63	—	—	0.60	0.69	0.64	0.61
	Img19	0.42	0.44	0.63	—	—	0.63	0.51	0.63	0.64
	Img20	0.46	0.44	0.57	—	—	0.64	0.55	0.61	0.64
	Mean	0.52	0.50	0.59	—	—	0.62	0.60	**0.63**	0.62
UIQM	Img15	3.67	2.86	4.87	4.65	4.54	4.29	4.08	5.21	4.51
	Img16	3.06	2.13	4.50	3.89	4.11	4.80	3.99	4.95	4.32
	Img17	1.85	4.18	5.36	5.18	5.08	4.63	4.49	5.31	5.74
	Img18	2.65	1.15	5.15	4.77	4.97	4.03	3.93	5.34	5.76
	Img19	2.64	1.01	4.42	4.24	4.04	4.73	4.15	4.98	4.66
	Img20	2.44	0.38	3.80	3.81	3.68	3.24	3.20	4.62	3.41
	Mean	2.72	1.95	4.69	4.42	4.40	4.29	3.97	**5.07**	4.73
AG	Img15	6.78	5.05	12.05	8.79	10.44	13.71	7.57	10.80	12.46
	Img16	4.12	3.10	7.68	4.71	6.01	8.45	4.50	6.70	7.47
	Img17	21.55	17.11	29.01	21.54	19.46	26.55	12.09	11.60	28.55
	Img18	11.12	8.47	15.92	10.96	5.58	13.75	8.18	11.02	16.87
	Img19	3.01	4.56	11.60	9.10	1.95	16.06	6.68	8.85	12.98
	Img20	2.89	2.90	6.44	5.20	1.14	12.40	5.61	6.07	9.77
	Mean	8.25	6.87	13.78	10.05	7.43	**15.15**	7.44	9.17	14.68
IE	Img15	5.37	3.02	6.04	6.50	4.96	5.83	8.89	4.46	5.80
	Img16	3.46	4.39	5.59	7.48	6.43	7.88	8.11	8.29	7.26
	Img17	6.07	1.01	7.58	1.02	1.24	7.65	7.63	8.92	7.95
	Img18	6.26	7.34	4.93	9.22	6.24	7.43	4.47	8.12	8.64
	Img19	0.99	3.39	5.00	5.66	2.55	7.51	7.56	3.96	7.39
	Img20	2.13	3.54	5.99	7.30	3.33	7.76	9.77	4.30	7.24
	Mean	4.05	3.78	5.85	6.20	4.12	7.34	**7.74**	6.34	7.38
PCQI	Img15	1.15	1.11	1.36	1.25	0.36	1.31	1.18	1.24	1.28
	Img16	0.98	1.07	1.38	1.16	0.43	1.34	1.18	1.25	1.29
	Img17	1.09	1.10	1.34	1.19	0.59	1.30	0.99	1.29	1.35
	Img18	1.07	1.13	1.39	1.20	0.48	1.35	1.13	1.33	1.39
	Img19	0.98	1.23	1.34	1.30	0.21	1.36	1.26	1.28	1.37
	Img20	1.08	1.17	1.19	1.17	0.25	1.22	1.14	1.16	1.22
	Mean	1.06	1.14	1.33	1.21	0.39	1.31	1.15	1.26	**1.32**

3.4 Ablation study

We performed ablation tests with the below combinations to verify the usability of each component of our strategy: (1) without contrast enhancement (CR) module, (2) without detail enhancement (DE) module and (3) without contrast enhancement (CE) module. As shown in Fig. 12, the CR module effectively solves color distortion problem of underwater images, regardless of blue, green, or yellow color casts. The absence of DE module leads to loss of image details, while the use of DE module successfully enhances image details and eliminates blurring artifacts. The exclusion of CE module reduces image clarity and contrast, whereas the use of CE module significantly improves image sharpness and contrast. The trial data demonstrate that our method is successful in visual quality, high contrast, and pronounced detail enhancement.

Most of the existing methods typically focus on one aspect, such as color restoration, contrast enhancement, or detail enhancement. These methods achieve local improvements in certain aspects but often cannot solve other degradation problems. Our method provides a comprehensive enhancement framework by combining contrast enhancement, color restoration, detail enhancement, and multi-scale fusion, which

solves multiple problems such as color distortion, low contrast, and blurry details. This multi-faceted enhancement method significantly improves the overall image quality, surpassing traditional single methods.

Furthermore, the ablation experiment clearly demonstrates the importance of each module:

1) Without CR module: The image exhibits significant color distortion.

2) Without DE module: The image lacks details and becomes blurry.

3) Without CE module: The contrast and clarity of the image decrease.

The final image (including all modules) presents the best color accuracy, detail enhancement, and contrast, proving that the combination of CR, DE, and CE modules is superior to that using any one method alone.

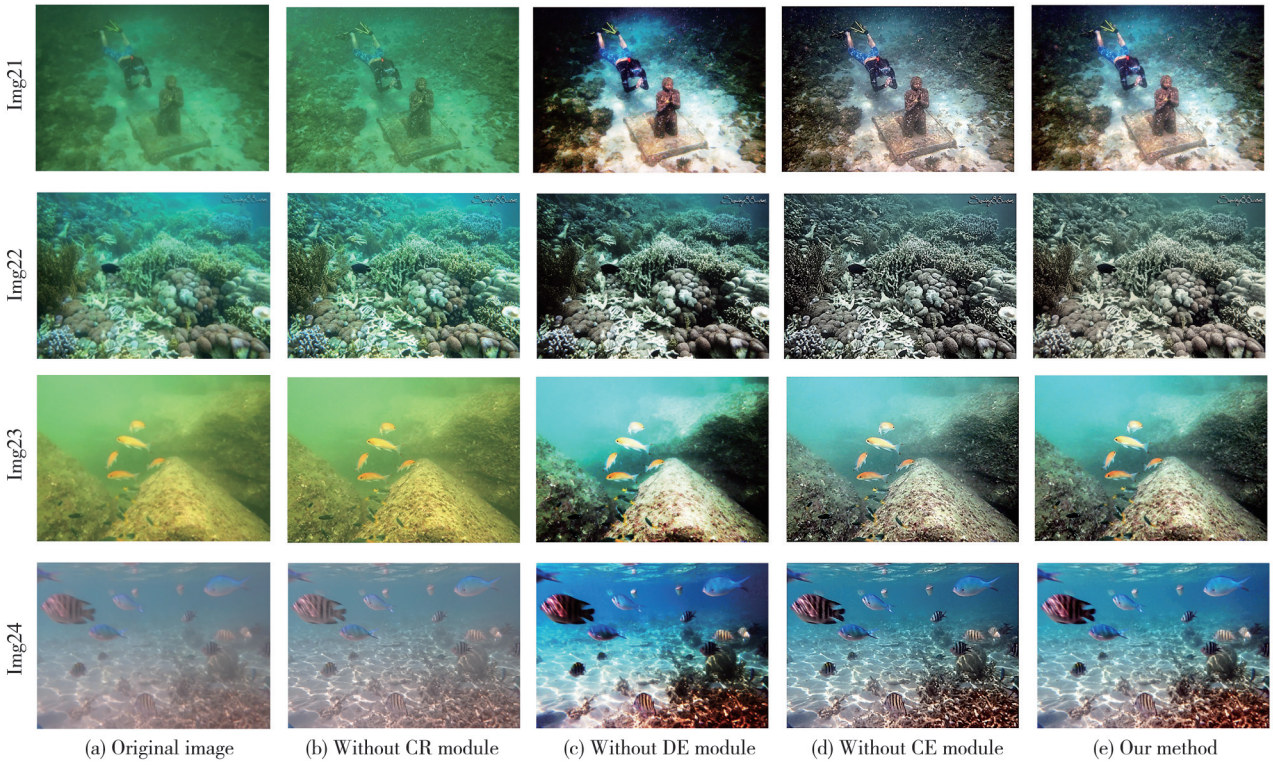

Fig. 12 Comparison of ablation results of different methods

3.5 Structural enhancement analysis

To further validate the effectiveness of our method in downstream applications such as object detection, we conducted additional verification using Canny edge detection.

Fig. 13 shows the results of Canny edge detection applied to the images enhanced by different algorithms.

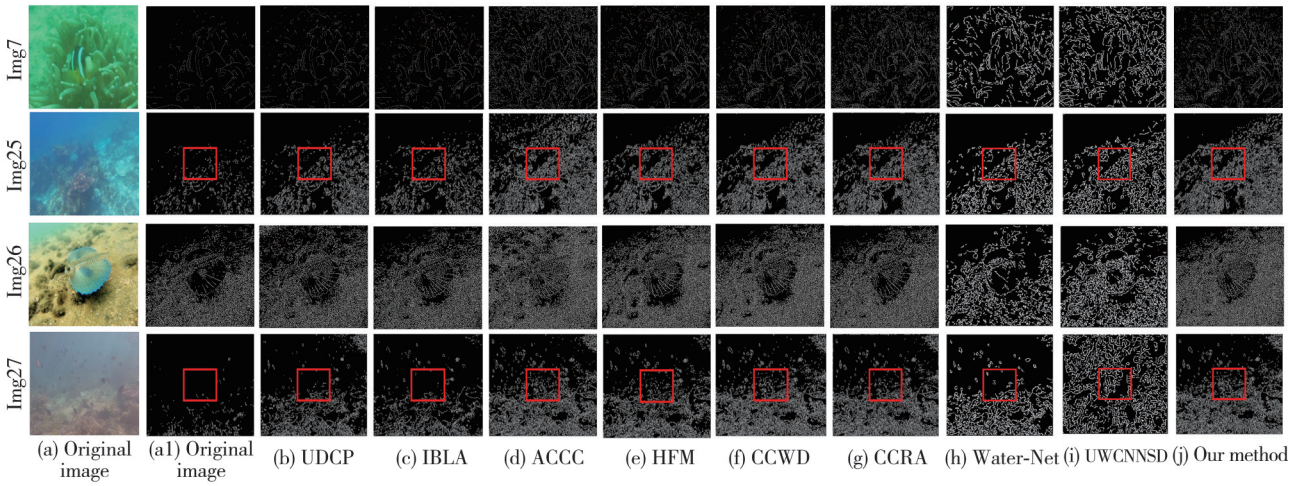

Fig. 13 Results of Canny edge detection

Compared with the existing methods, our algorithm significantly increases the number of detectable edges and reveals richer edge details, thereby improving edge detection accuracy.

3.6 Efficiency experiment

To better demonstrate the advantages and limitations of our method, we conducted a comprehensive evaluation of computational efficiency, including the processing time required. We have tested on the following hardware configurations: CPU, Intel (R) Core (TM) i7-10700, and GPU, RTX 2060. For traditional methods (UDCP, IBLA, ACCC, HFM, CCWD, CCRA, and our method), they were tested in Matlab environment using CPU. For deep learning-based methods (Water-Net, UWCNN-SD), GPU testing was conducted in a Python environment. The test results are shown in Table 5. It can be seen that although our method does not reach the optimal value in terms of efficiency, image quality is also an important evaluation indicator as well as real-time performance.

Table 5 Efficiency information of different methods

Method	Hardware	Time/s
UDCP	CPU	38.11
IBLA	CPU	33.45
ACCC	CPU	16.37
HFM	CPU	45.27
CCWD	CPU	7.54
CCRA	CPU	33.45
Water-Net	GPU	0.03
UWCNN-SD	GPU	0.40
Our method	CPU	18.53

Note: The runtime comes from different hardware environments and is only of reference value. It should not be regarded as an accurate comparison under equal conditions.

3.7 Generalization experiment

The generalization experiment shows that our method has good enhancement ability for underwater images and has good generalization ability not only for underwater images but also for dancing images and low illumination images. As shown in Fig.14, it is better at removing fog from foggy images and significantly improves the brightness and contrast of low light images.

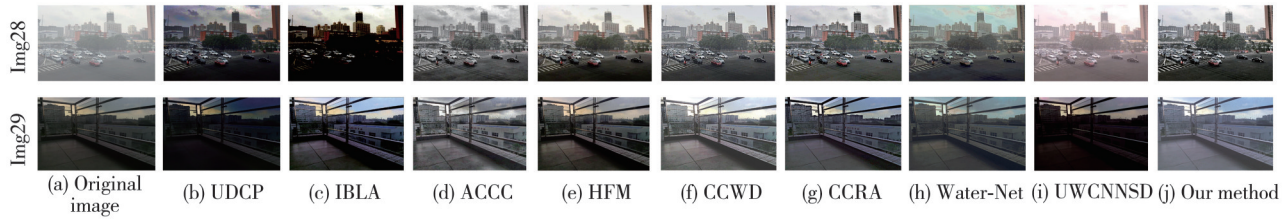

Fig. 14 Enhancement results of different methods for fog and low-light images

4 Conclusions

To address issues such as color distortion, detail blurring, and low contrast in underwater degraded images, we propose a multi-scale fusion based underwater image enhancement algorithm. Instead of relying on complex underwater optical imaging models, our method leverages different visual characteristics of single images for image enhancement. The method consists of four main stages: 1) color compensation based on dark-bright channel processing, 2) detail enhancement utilizing morphological transformations, 3) contrast improvement employing BEO algorithm, and 4) multi-scale fusion for underwater image enhancement.

Extensive experimental analysis demonstrates the effectiveness and robustness of the proposed algorithm, with good performance in quantitative metrics. Furthermore, our method shows potential for supporting subsequent underwater imaging applications such as object detection. However, this method introduces red artifacts when processing images with severe green color casts, which requires further improvement in future work.

Acknowledgement

The work was supported by National Natural Science Foundation of China (No. 12401703), Natural Science Foundation of Shanxi Province (No.202403021212256), and the 20th Graduate Science and Technology Project of North University of China (No.20242042).

Declaration of conflicting interests

The authors have no conflict of interest related to this publication.

References

[1] RAVEENDRAN S, PATIL M D, BIRAJDAR G K. Underwater image enhancement: a comprehensive review, recent trends, challenges and applications. Artificial Intelligence Review, 2021, 54(7): 5413-5467.

[2] WANG Y, SONG W, FORTINO G, et al. An experimental-based review of image enhancement and image restoration

methods for underwater imaging. IEEE Access, 2019, 7: 140233-140251.
[3] FAYAZ S, PARAH S A, QURESHI G J, et al. Underwater image restoration: a state-of-the-art review. IET Image Processing, 2021, 15(2): 269-285.
[4] PENG Y T, COSMAN P C. Underwater image restoration based on image blurriness and light absorption. IEEE Transactions on Image Processing, 2017, 26(4): 1579-1594.
[5] ZHANG M H, PENG J H. Underwater image restoration based on a new underwater image formation model. IEEE Access, 2018, 6: 58634-58644.
[6] LI H Y, WANG H, ZHANG Y, et al. Underwater image captioning: Challenges, models, and datasets. ISPRS Journal of Photogrammetry and Remote Sensing, 2025, 220: 440-453.
[7] JAFFE J S. Computer modeling and the design of optimal underwater imaging systems. IEEE Journal of Oceanic Engineering, 1990, 15(2): 101-111.
[8] NARASIMHAN S G, NAYAR S K. Contrast restoration of weather degraded images. IEEE Transactions on Pattern Analysis and Machine Intelligence, 2003, 25(6): 713-724.
[9] HE K M, SUN J, TANG X O. Single image haze removal using dark channel prior//2009 IEEE Conference on Computer Vision and Pattern Recognition, June 20-25, 2009, Miami, FL, USA. New York: IEEE, 2009: 1956-1963.
[10] GALDRAN A, PARDO D, PICÓN A, et al. Automatic Red-Channel underwater image restoration. Journal of Visual Communication and Image Representation, 2015, 26: 132-145.
[11] DREWS P L J, NASCIMENTO E R, BOTELHO S S C, et al. Underwater depth estimation and image restoration based on single images. IEEE Computer Graphics and Applications, 2016, 36(2): 24-35.
[12] DREWS P Jr, DO NASCIMENTO E, MORAES F, et al. Transmission estimation in underwater single images//2013 IEEE International Conference on Computer Vision Workshops, December 2-8, 2013, Sydney, NSW, Australia. New York: IEEE, 2014: 825-830.
[13] LIANG Z, DING X Y, WANG Y F, et al. GUDCP: generalization of underwater dark channel prior for underwater image restoration. IEEE Transactions on Circuits and Systems for Video Technology, 2022, 32(7): 4879-4884.
[14] AHMAD AWAN H S, MAHMOOD M T. A nonconvex approach with structural priors for restoring underwater images. Mathematics, 2024, 12(22): 3553.
[15] REZA A M. Realization of the contrast limited adaptive histogram equalization (CLAHE) for real-time image enhancement. Journal of VLSI Signal Processing Systems for Signal, Image and Video Technology, 2004, 38(1): 35-44.
[16] CARDEI V C, FUNT B, BARNARD K. White point estimation for uncalibrated images. Color and Imaging Conference, 1999, 7(1): 97-100.
[17] LAND E H, MCCANN J J. Lightness and retinex theory. Journal of the Optical Society of America, 1971, 61(1): 1.
[18] ANCUTI C O, ANCUTI C, DE VLEESCHOUWER C, et al. Color balance and fusion for underwater image enhancement. IEEE Transactions on Image Processing, 2018, 27(1): 379-393.
[19] LIN S J, LI Z, ZHENG F H, et al. Underwater image enhancement based on adaptive color correction and improved retinex algorithm. IEEE Access, 2023, 11: 27620-27630.
[20] WANG Z B, ZHOU D J, LI Z C, et al. Underwater image enhancement via adaptive color correction and stationary wavelet detail enhancement. IEEE Access, 2024, 12: 11066-11082.
[21] AN S M, XU L H, DENG Z C, et al. HFM: a hybrid fusion method for underwater image enhancement. Engineering Applications of Artificial Intelligence, 2024, 127: 107219.
[22] ZHANG W D, WANG Y D, LI C Y. Underwater image enhancement by attenuated color channel correction and detail preserved contrast enhancement. IEEE Journal of Oceanic Engineering, 2022, 47(3): 718-735.
[23] ANWAR S, LI C Y. Diving deeper into underwater image enhancement: a survey. Signal Processing: Image Communication, 2020, 89: 115978.
[24] GU J X, WANG Z H, KUEN J, et al. Recent advances in convolutional neural networks. Pattern Recognition, 2018, 77: 354-377.
[25] LI C Y, GUO C L, REN W Q, et al. An underwater image enhancement benchmark dataset and beyond. IEEE Transactions on Image Processing, 2020, 29: 4376-4389.
[26] WU S C, LUO T, JIANG G Y, et al. A two-stage underwater enhancement network based on structure decomposition and characteristics of underwater imaging. IEEE Journal of Oceanic Engineering, 2021, 46(4): 1213-1227.
[27] FU Z Q, WANG W, HUANG Y, et al. Uncertainty inspired underwater image enhancement//Computer Vision – ECCV 2022. Cham: Springer Nature Switzerland, 2022: 465-482.
[28] Li J, Skinner K A, Eustice R M, et al. WaterGAN: Unsupervised generative network to enable real-time color correction of monocular underwater images. IEEE Robotics and Automation letters, 2018, 3(1): 387-394.
[29] WANG Z F, LI C F, MO Y Z, et al. RCA-CycleGAN: Unsupervised underwater image enhancement using red channel attention optimized CycleGAN. Displays, 2023, 76: 102359.
[30] ZHANG H B, SAN H J, CHEN J P, et al. Black eagle optimizer: a metaheuristic optimization method for solving engineering optimization problems. Cluster Computing, 2024, 27(9): 12361-12393.
[31] YUAN J Y, CAO W, CAI Z C, et al. An underwater image vision enhancement algorithm based on contour Bougie morphology. IEEE Transactions on Geoscience and Remote Sensing, 2021, 59(10): 8117-8128.
[32] Gonzalez RC, Woods R. Digital image processing: Pearson education india, 2009.
[33] YANG C C. Image enhancement by modified contrast-stretching manipulation. Optics & Laser Technology, 2006, 38(3): 196-201.

[34] KARAKAYA D, ULUCAN O, TURKAN M. Pas-mef: multi-exposure image fusion based on principal component analysis, adaptive well-exposedness and saliency map// ICASSP 2022 - 2022 IEEE International Conference on Acoustics, Speech and Signal Processing, May 23-27, 2022, Singapore, Singapore. New York: IEEE, 2022: 2345-2349.

[35] GUO Y T, HU H P, YANG Z M. Low light image enhancement based on multi-scale fusion. Journal of Test and Measurement Technology, 2025, 39(3): 322-329.

[36] LIU R S, FAN X, ZHU M, et al. Real-world underwater enhancement: challenges, benchmarks, and solutions under natural light. IEEE Transactions on Circuits and Systems for Video Technology, 2020, 30(12): 4861-4875.

[37] BUCHSBAUM G. A spatial processor model for object colour perception. Journal of the Franklin Institute, 1980, 310(1): 1-26.

[38] XIONG N N, SHEN Y, YANG K Y, et al. Color sensors and their applications based on real-time color image segmentation for cyber physical systems. EURASIP Journal on Image and Video Processing, 2018, 2018(1): 23.

[39] JANG W, SON K, KIM J, et al. Auto white balance system using adaptive color samples for mobile devices//APCCAS 2008 - 2008 IEEE Asia Pacific Conference on Circuits and Systems, November 30 - December 3, 2008, Macao, China. New York: IEEE, 2009: 1462-1465.

[40] ZHANG L J, LIU T N, SHI Q C, et al. Underwater image enhancement based on depth and light attenuation estimation. IET Image Processing, 2025, 19(1): e70037.

[41] LV S, ZHANG W X, ZHANG M H, et al. Underwater binocular 3D imaging method based on polarization difference ghost imaging. Optics and Lasers in Engineering, 2025, 186: 108856.

[42] XUE Q Q, HU H P, BAI Y P, et al. Underwater image enhancement algorithm based on color correction and contrast enhancement. The Visual Computer, 2024, 40(8): 5475-5502.

[43] HSIEH Y Z, CHANG M C. Underwater image enhancement and attenuation restoration based on depth and backscatter estimation. IEEE Transactions on Computational Imaging, 2025, 11: 321-332.

[44] WANG S Q, MA K D, YEGANEH H, et al. A patch-structure representation method for quality assessment of contrast changed images. IEEE Signal Processing Letters, 2015, 22(12): 2387-2390.

基于颜色、细节、对比度协同优化和多尺度融合的水下图像增强

曹　瑞，李　波，胡红萍*，张振伟，朱鑫婵

中北大学 数学学院，山西 太原 030051

摘　要：由于光在水中的吸收和散射，水下图像通常会出现色移、低可见度和细节模糊等退化现象。针对这些问题，提出了一种颜色、细节、对比度和多尺度融合的水下图像增强算法。首先使用基于暗通道和亮通道的颜色恢复方法来校正水下图像的颜色失真，恢复其自然的颜色平衡。其次，利用形态学运算增强图像中物体的轮廓和结构信息，以提高细节表示。此外，引入了黑鹰优化算法，并设计了一种新的适应度函数来自适应优化图像对比度。在融合阶段，提出了主成分权重，并将其与其他加权策略相结合，实现了多尺度图像信息融合，在保持丰富纹理和细节的同时增强了对比度。在两个真实的水下图像数据集UIEB和RUIE上的实验结果表明，与现有方法相比，该算法有效地减少了退化现象，提升了图像颜色保真度、对比度和细节清晰度。客观分析显示该方法在UCIQE、UIQM、AG、IE、PCQI等方面也优于其他相关方法。本研究为水下图像处理技术提供了参考。

关键词：水下图像；色彩恢复；形态学变换；黑鹰优化算法；主成分权重；多尺度融合

引用格式：CAO Rui, LI Bo, HU Hongping, et al. Underwater image enhancement through cooperative optimization of color, detail, contrast and multi-scale fusion. Journal of Measurement Science and Instrumentation, 2026, 17(1): 97-113. DOI: 10.62756/jmsi.1674-8042.2026008